2008 IEEE International Conference on
Robotics and Automation
Pasadena, CA, USA, May 19-23, 2008

Rolling Mechanical Imaging: A Novel Approach for Soft Tissue Modelling and Identification during Minimally Invasive Surgery

Hongbin Liu, David P. Noonan, Kaspar Althoefer, Lakmal D. Seneviratne

Abstract—**This paper proposes a novel approach for the identification of the internal structure and mechanical properties of biological soft tissue using a force sensitive wheeled probe to generate a 'mechanical image' by rolling across the surface of a solid organ. Initially, a testing facility for validating the concept ex-vivo was developed. Preliminary validation tests were carried out on a silicone phantom with embedded abnormalities with the aim to link the derived 'mechanical image' with the known internal structure. *Ex-vivo* validation tests were also conducted on excised porcine livers. The data were analyzed in four parts: 1) the dynamic analysis of wheel-tissue interaction to validate that the measured parameters are representative of underlying tissue stiffness; 2) the development of a 'mechanical image' from the rolling data; 3) a comparison of standard 1-DOF indentation testing with 2-DOF rolling and 4) the characterization of the relationship between Force and Tissue Deflection from the data contained within the mechanical image. The results show that the 'rolling mechanical image' is capable of capturing information relating to the underlying tissue stiffness distribution and characterizing the Force-Tissue Deflection profile for a tissue sample. Examples of scenarios, where this information could potentially be used, include providing a surgeon with the ability to probe solid organs *in-vivo* during robot-assisted MIS or providing prior information for the modeling of tool-tissue interactions, such as steerable needles.**

I. Introduction

THIS paper presents work carried out to develop a force sensitive wheeled probe capable of identifying both tissue parameters and abnormalities during Minimally Invasive Surgery (MIS). The purpose is to provide a surgeon with the ability to mechanically probe a large area of solid organs within a short time and thus classify tissue properties and identify abnormalities. Existing techniques aim to identify tissue properties via force measurement from 1-DOF probing [1-3], grasping [4] or stretching of a tissue sample [5] or via a tactile sensor array pressed onto the surface of the tissue [6-8]. While these approaches are effective in a localized setting, their efficacy is impaired due to the inherently variable nature of biological soft tissue. In order to effectively identify tissue properties, or more importantly to indicate the presence of an underlying abnormality, a large area of an organ must be examined. With the aforementioned techniques this can be impractical due to the size restrictions associated with MIS, the time it takes to probe a large area and inconclusive data as a result of changing boundary conditions. In this paper we present the ex-vivo validation and analysis of a device which has the ability to perform a large area characterization in a reduced time by rolling over an organ's surface while recording the force response of the tissue with a force-sensitive wheeled probe. By rolling over multiple paths at specific indentation depths and stitching individual force profiles together a 'mechanical image' indicating the underlying tissue stiffness distribution can be generated. Furthermore, through increasing the indentation depth over successive passes, an assembly of mechanical images can be obtained. These can then be analyzed to extract information relating to the Force-Tissue Deflection characteristic of the tissue sample.

This novel 'rolling' approach to soft tissue property identification differs from existing techniques in that it utilizes a force-sensitive wheeled probe to generate a mechanical image and Force-Deflection characteristic of the underlying tissue sample. This ability to measure the temporal and spatial variation of the force signal can overcome some of the disadvantages associated with current techniques.

Manuscript received September 15, 2006.

H. Liu, D. Noonan, K. Althoefer, L. D. Seneviratne are with the King's College London, Mechanical Engineering Department, Strand, London, WC2R 2LS, UK (e-mail:{ hongbin.liu, david.noonan, k.althoefer, lakmal.seneviratne} @kcl.ac.uk)

II. Background

A. Minimally Invasive Surgery

The Minimally Invasive Surgery (MIS) refers to surgeries performed through small incisions. Its benefits include reduced patient trauma and blood loss as well as decreased recovery time and the associated hospitalisation costs [9]. A procedure is performed by passing a laparoscope, to provide an imaging field of view, and various other laparoscopic instruments through a trocar port. However, advantages of MIS are offset by the sharp increase in the technical difficulty associated with the approach. Firstly, the surgeon's ability to both see and touch the operating environment is reduced. Secondly, distal dexterity is also impaired due to use of long, rigid instruments introduced through a fixed point [10]. This reduction of visual, haptic and tactile feedback coupled with dexterity problems can lead to accidental damage of tissue [11].

Several robotic systems have been developed to overcome some of these problems. However, while existing systems, such as the daVinci Surgical System™ from Intuitive Surgical, do offer improvements by providing a stereoscopic view of the operative field, enhanced distal dexterity at the instrument tip and an ergonomic operating position, the ability of a surgeon to recover information regarding tissue properties or to 'feel' any forces *in-vivo* is still notably

absent [12]. Investigation into techniques which can overcome this limitation, and thus improve a surgeon's ability to perform both diagnostic and therapeutic interventions, is an ongoing research problem.

B. Mechanical Imaging

One subset of this research is that of 'Mechanical Imaging'. This is a new technology of medical diagnostics in which internal structure of soft tissue is visualized by sensing the mechanical stresses on the surface of an organ using a tactile sensor array [6]. In contrast to other existing imaging modalities which use sophisticated hardware such as MRI or CT, current mechanical imaging devices only require a tactile sensor array and a positioning system. There are currently two applications of such a device being developed - for the diagnoses of breast and prostate cancer. In both of these cases palpation has proven to be an effective method for detecting and monitoring pathological changes. Wellman et al. [7] applied tactile mechanical imaging to compare a nodule size estimate from preoperative physical examination, ultrasound and tactile imaging with the postoperative measurement of the resected nodules. The results showed that the tactile imaging had good repeatability and less error (13%) than other methods with respect to the resected measurements. Egorov et al. [8] have developed the 'prostate mechanical imager' for the real-time imaging of prostate using a transrectal probe equipped with a pressure sensor array and position tracking sensor. This device has been validated in laboratory experiments on prostate phantoms and in a clinical study. While the results from both cases illustrate that tactile sensor arrays have potential as diagnostic tools, their adaptation to the MIS is problematic due to the problems associated with miniaturization and sterilization. The force-sensitive wheeled probe presented in this paper can be easily miniaturized and sterilized and is capable of generating 'rolling mechanical images' over a large surface area in a short period of time.

III. Wheeled Probe Testing Facility

The testing facility is required to allow for controlled movement of the wheel across the surface of a soft tissue sample. To facilitate this, a wheeled probe was constructed and attached to the distal tip of a Mitsubishi RV-6SL 6-DOF robotic manipulator. An ATI NANO17 Force/Torque sensor (SI-12-0.12 with 16-bit DAQ (NI PCI 6034E)) was mounted between the wheeled probe and the manipulator distal tip so as to allow for the measurement of the three force components (F_x, F_y, F_z) imparted by the tissue onto the wheel, as shown in Fig. 1.

A trocar port compatible aluminium wheel (diameter 8mm, width 8mm) was used as the end-effector. The wheel was grooved with 12 teeth to avoid slip during rolling and mounted 1n the 'ball bearing 1' as shown in Fig. 1. The shaft connecting the wheel to the sensor was mounted in the 'ball bearing 2' to permit axial rotation, thus allowing the probe to follow curved trajectories in the x-y plane. A 2mm offset between the center of the wheel and the axis of the force sensor provides sufficient torque to rotate the probe when the manipulator adjusts its trajectory.

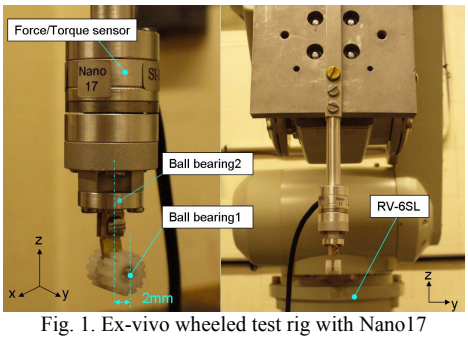

Fig. 1. Ex-vivo wheeled test rig with Nano17

IV. Rolling Mechanical Imaging from Silicone Phantom

A. Silicone Phantom Test Block with Hard Nodules

Preliminary tests to gauge the efficacy of the wheeled probe at identifying underlying areas of tissue internal structure were carried out using a silicone phantom. The intention of this approach is to link the rolling mechanical imaging with the known ground truth data from the phantom internal structure. The liver is a vascular, solid organ with large amount of hepatic arteries and veins making it extremely difficult to acquire the internal configuration of the tissue sample for comparison to the measured mechanical imaging under laboratory conditions. Therefore a silicone phantom suitable for soft tissue simulation (RTV6166, General Electric [13]) with six simulated rubber nodules was constructed. The dimensions of the phantom and the nodules are shown in Fig. 2. The main mechanical properties of the silicone and rubber are listed in Table I.

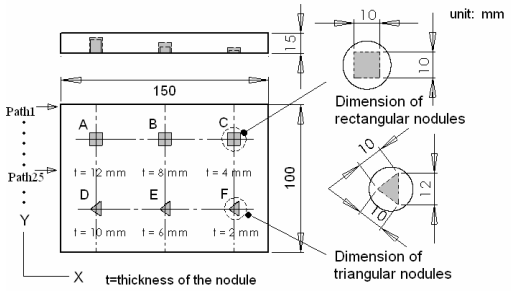

Fig. 2. The dimension of the silicone phantom displaying location, shape and depth of the six simulated nodules (A-F), each with a thickness, *'t'*

TABLE I
MECHANICAL PARAMETERS OF THE SILICONE PHANTOM

	Elastic Modulus (Pa)	Poisson's Ratio	Shear Modulus (Pa)	Mass Density (kg/m^3)
Rubber	$8.7x10^6$	0.49	$2.9x10^6$	1000
Silicone	$4.9x10^5$	0.45	$1.63x10^5$	2200

To generate the mechanical image of the internal structure of the silicone model a series of 50 paths parallel to the x axis were defined, with a shift of 2mm along the y axis between paths. The force imparted by the sample onto the wheel, as measured by the Force/Torque sensor, was recorded during each traverse. These multiple force profiles

were then stitched together to generate a 'rolling mechanical image' using *Matlab*. The image projects the geometry of stiffness distribution of the rolling area into an x-y plane. This procedure was repeated for indentation depths of 2mm, 3mm and 4mm.

B. *Results from Silicone Phantom*

It was found that the high force intensity recorded from the square nodules effectively eclipses the response from the triangular nodules. To compensate for this, the original results are split into two parts: Part 'I', showing the result for the square nodules (A-C) and Part 'II, showing the result for the triangular nodules (D-F). The rolling images resulting from this approach are shown in Fig. 3.

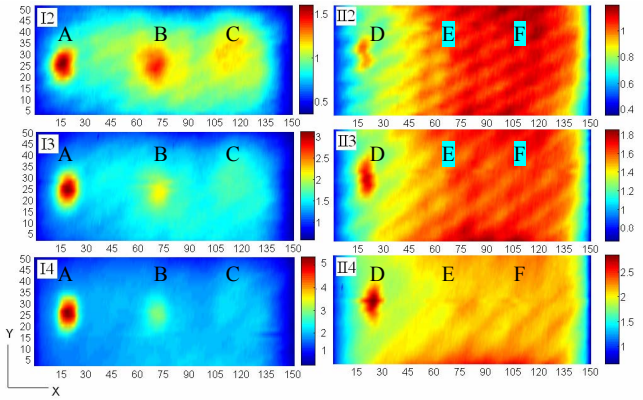

Fig. 3. The rolling mechanical images from the silicone phantom with embedded nodules showing *(left)* Part I and *(right)* Part II. I_i or II_i (i=2, 3, 4) represents the rolling image of the respective Part with an indentation depth of *i mm.* The unit of color bars is in 'Newton'.

Fig. 3 shows that nodules A, B, D are clearly visible at all rolling indention depths and their locations on the rolling image are consistent with their counterparts in the silicone phantom. However, nodules C, E and F can not be conclusively identified at any indentation depth as, with less thickness, *t*, than the other three nodules, they display less force responses when traversed by the wheeled probe.

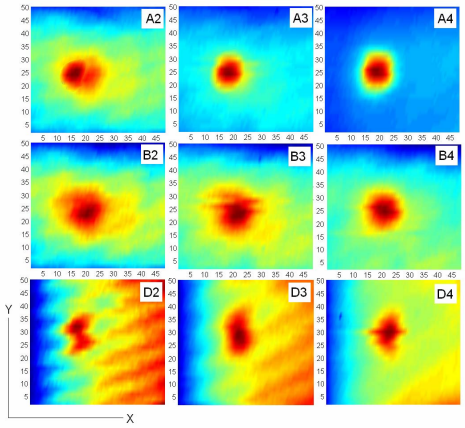

Fig. 4. The rolling mechanical image of nodule A, B, D. A_i (B_i, D_i) represents the rolling image of nodule A (B, D) from the test with *i* mm indentation depth.

In order to measure the ability of the rolling imaging to document the size and shape of the nodules, images of the visible nodules were extracted from Fig. 3. Using the *Matlab Image Processing Toolbox*, their x-y surface area indicated on rolling images, as a percentage difference to the physical nodule x-y surface area, was calculated as shown in Table II. It can be seen from Fig. 4, the rolling image can differentiate the shape of square (A) and triangle (D) at 4mm rolling indentation depth, and the accuracy of rolling image improves as the indentation depth increases. These results show that the rolling mechanical image can be used to identify the location and the approximate shape and size of abnormalities buried inside a simulated soft tissue sample. However, further work is required to investigate how sensitive it is to changes in indentation depth, nodule depth and nodule thickness.

TABLE II
THE DIFFERENCE BETWEEN NODULE'S SURFACE AREA INDICATED ON THE ROLLING IMAGE AND THE ACTUAL PHYSICAL SURFACE AREA

Indentation depth of test	2mm	3mm	4mm
Nodule A	75%	14%	26%
Nodule B	136%	129%	71%
Nodule D	NA	88%	30%

V. EX-VIVO TESTS WITH PORCINE LIVER

While silicone phantom tests are useful for preliminary characterization, due to widely varying testing and boundary conditions it is essential to perform tests with biological soft tissue ex-vivo to investigate the efficacy of the 'rolling mechanical imaging' technique before moving towards in-vivo experiments. Key differences between silicone and tissue include an uneven, slick surface which presents difficulties in maintaining a constant indentation depth, avoiding wheel slip and the accurate measurement of normal force response. Each of these issues must be addressed in order to obtain accurate ex-vivo results. For the purposes of this paper, ex-vivo investigation of the efficacy of the wheeled probe was conducted on three excised porcine liver samples. The characteristics of liver samples and testing environments are listed in Table III. In each test, one of the livers' lobes was fixed to a polyethylene foam bed (52mm in thickness, Young's modulus = 10.6 MPa) using 8~10 pins to prevent the tissue sliding under the translational loading from the robot manipulator. A rectangular testing area 600mm^2 was chosen. Its approximate location on one of the liver samples is highlighted by a dashed frame in Fig. 5.

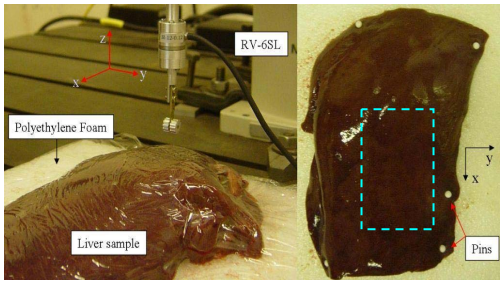

Fig. 5. The setting for ex vivo Porcine Liver tests. 8~10 pins were used to fix the left lobe of a porcine liver onto the polyethylene foam.

The first stage was to pre-experimentally perform surface registration of the tissue sample for the purpose of using

prior knowledge of the tissue topographical structure to maintain a constant indentation depth while traversing its surface. The surface registration was performed by defining eight paths parallel to the *x* axis, each separated by 8mm along the positive *y* axis. Each of these paths was then split into ten waypoints. At each waypoint the height of the tissue surface was visually determined by advancing the probe along the *z*-axis until full wheel contact occurred. The result was a mesh of 80 points representing the surface topography of the liver. During the surface registration, a plastic cling film of negligible thickness was used to cover the entire lobe to prevent loss of water content. Fig. 6 shows the surface registration of one liver sample. Solid dots indicate the predefined waypoints and the dashed lines represent those 8 rolling paths.

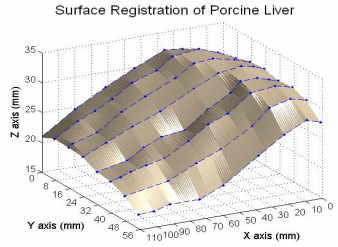

Fig. 6. The surface registration of a porcine liver by setting 80 waypoints in the testing area

TABLE III
THE CHARACTERISTICS OF TISSUE SAMPLES & TESTING CONDITIONS

Porcine livers	Weight (kg)	Temp.(°C) / Humidity(%)	Selected lobe(s)
Liver A	1.35	23 / 23	Left central lobe
Liver B	1.75	24.1 / 40	Left central lobe
Liver C	2.20	24.4 / 33	Right lateral lobe

VI. DYNAMIC ANALYSIS OF LIVER ROLLING TESTS

The rolling experiments were conducted on Liver A and Liver B. The rolling tests were firstly to study the dynamics of rolling wheel-tissue interaction. Secondly, force responses recorded during the tests were used to generate the rolling mechanical image of the underlying tissue structure of each liver. During these tests the wheel was rolled over the surface with a fixed indentation depth. This depth was then varied from 1mm to 6mm in 1mm increments. This was repeated three times for each indentation depth. The translational speed of the wheel during tests was 15mm/s.

Researchers have divided the resultant force between a wheel and soft tissue into three force components; the membrane force, the shear force and pressure force [14]. However the parameters required to implement this model include the viscosity of the peritoneal fluid and simultaneous fore and aft wheel contact angles – all of which are difficult to measure. For the purpose of this preliminary study, the rolling force is simplified as only consisting of the normal force and the tangential force, the identification of which only requires force-vector measurement and surface registration of the soft tissue. As shown in the force diagram Fig. 7: 1) T is the translational direction of the wheel, which is defined as the tangential direction at the wheel-tissue contact point; 2) θ is the angle between T and the x-axis and it can be calculated using the aforementioned 3D surface registration map; 3) F_x, F_y, F_z are the three orthogonal force components as measured by the F/T sensor; 4) F_r is the resultant force of F_x, F_y, F_z; 5) F_{xy} is the resultant force of F_x and F_y.

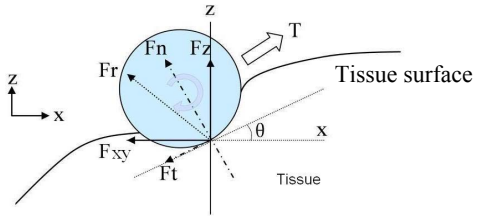

Fig. 7.The force diagram of the wheel-soft tissue rolling interaction

The simultaneous tangential force (F_t) and normal force (F_n) then can be derived using the following equations:

$$F_t = F_{xy} \cdot \cos\theta - F_z \cdot \sin\theta$$
$$F_n = F_{xy} \cdot \sin\theta + F_z \cdot \cos\theta \quad (1)$$

By applying Eq.1 to the experimental data from Liver A and Liver B, the simultaneous tangential forces and normal forces at the 80 predefined waypoints were acquired. The results, summarized in Table IV and Fig. 8, show that the T/N ratio (ratio of tangential force over the normal force) and the N/R ratio (ratio of rolling normal force over the resultant force) remain relatively constant despite variations in both the rolling indentation depth and the rolling-normal and resultant forces. Moreover the T/N ratio is small (~0.2) and N/R ratio is very close to 1 (~ 0.98). The high N/R ratio indicates that the normal force predominates the force signal and hence it can be expected that the information contained in the force signal is primarily from the stiffness of the underlying soft tissue rather than the shear force and membrane force. In another word, the rolling method can be used to examine the stiffness distribution of a soft tissue sample if the wheel-slip issue can be effectively eliminated. As was mentioned in Section III, this was achieved by placing a series of 12 grooves in the wheel.

TABLE IV
THE T/N AND N/R RATIOS FROM DIFFERENT ROLLING INDENTATION DEPTH

Rolling Indentation Depth	Liver A		Liver B	
	T/N	N/R	T/N	N/R
6 mm	0.239	0.972	0.198	0.980
5 mm	0.221	0.976	0.176	0.984
4 mm	0.214	0.977	0.162	0.987
3 mm	0.213	0.978	0.161	0.987
2 mm	0.208	0.978	0.142	0.990

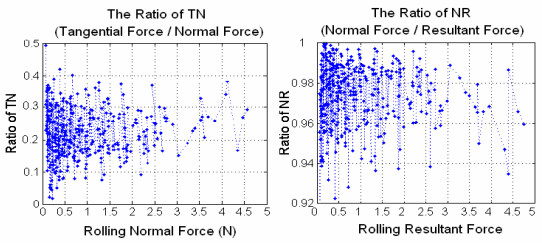

Fig. 8. The T/N ratio vs. the Rolling Normal Force; the N/R ratio vs. Rolling Resultant Force. This data contains 6 rolling tests conducted on Liver A with rolling indentation depth varied from 2 to 6mm

VII. Soft Tissue Modelling Basing on Rolling Mechanical Imaging

A. Development of a 'Rolling Mechanical Image'

The force sensitive wheeled probe was rolled across large areas of the organ's surface using multiple paths at a certain indentation depths and the resulting individual force profiles were stitched together to develop the 'rolling mechanical image'. By changing indentation depth incrementally (from 1mm to 6mm), an assembly of images from different indentation depths was obtained (see Fig. 9).

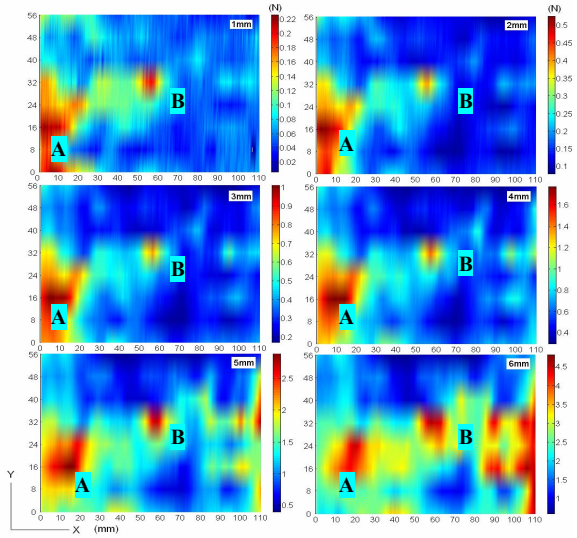

Fig. 9. The geometry of stiffness distribution of Liver B. The stiffness distribution is projected onto x-y plane from 1mm rolling indentation depth to 6mm (the unit of color bars is in 'Newton')

The assembly of rolling mechanical images indicates both the geometry of stiffness distribution and the corresponding stiffness development as the tissue deformation increases. Its unstructured appearance is representative of the nature of the organ – highly vascular with hepatic arteries and veins. Without imaging modalities such as CT or MR imaging it is very difficult to link any of the areas of increased stiffness observed in Fig. 9 to actual features inside the liver. However, what the image does show is that this organ has two repeatable areas of increased stiffness – a large area in the lower left hand corner of the image (A) and a small, isolated area near the centre of the image (B). During testing, both of these areas of stiffness were clearly identifiable by palpating the organ by hand. However, during robot-assisted MIS the ability of a surgeon to perform such a procedure is absent. We propose that this novel approach of intra-operatively providing surgeon with large area 'rolling mechanical image' of solid organs using a wheeled probe could be utilized to improve their ability to make diagnostic and interventional decisions.

B. 1-DOF Indentation Tests vs.2-DOF Rolling Tests

As we have shown in previous work [15, 16] 1-DOF indentation can be used to identify underlying tissue parameters relating to tissue viscoelasticity. However, the normal force response recorded during such tests is not immediately comparable to the rolling-normal force, as the dynamic effect of rolling over soft tissue is a much more complex interaction.

In order to investigate the relationship between the rolling normal force and the normal force from a series of discrete 1-DOF indentations, an additional set of experiments were performed on 'Liver C' using the information collected during the earlier surface registration. In this case a 1-DOF indentation was made at each of the 80 points used to define rolling paths and the force at each point recorded. The indentation depth was initially set to 1mm and increased in 1mm increments to 6mm. To avoid preconditioning the tissue, it was allowed to recover for 4 minutes between tests, at which time it was again covered with cling film to avoid dehydration. When aligned with the rolling results, this now presents two complementary data sets – one representing a continuous distribution along the pre-defined paths and the other representing multiple discrete force measurements along the same paths. By plotting the 1-DOF indentation forces at each of the 80 points and sampling the rolling normal forces at the same 80 points, it was found that the rolling-normal force was consistently higher. This is to be expected due to the additional shear and membrane forces experienced during rolling. Moreover, as shown in Fig. 10, defining F_{in} as the 1-DOF indentation force and F_n as the rolling-normal force, the ratio between them (IN_{ratio}) can be described as a linear function of the rolling-normal force given by:

$$IN_{ratio} = \frac{F_{in}}{F_n} = P_1 F_n + P_2 \qquad (2)$$

Under these testing conditions, P_1 = *-0.04*, P_2= *0.58*. By letting $F_n = \varepsilon F_{ro}$, where ε represents the N/R ratio (can be found in Table IV), F_{ro} is the rolling-resultant force, the relationship between F_{in} and F_{ro} can be expressed as:

$$F_{in} = \varepsilon F_{ro}(\varepsilon F_{ro} P_1 + P_2) \qquad (3)$$

It was found that the IN_{ratio} maintained similarity when calculated at different indentation depths, as can be seen in Table V (mean = 0.5394, SD (Standard Deviation) = 0.019). This indicates that the ratio of 1-DOF indentation force over rolling normal force is independent of indentation depth and represents an important first step in extracting viscoelastic parameters from a rolling mechanical image.

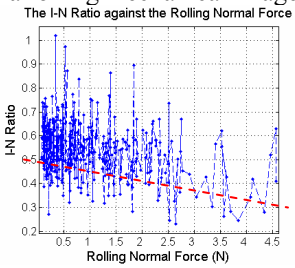

Fig. 10. The IN ratio against the rolling-normal force. The dashed line shows the decreasing linear relationship

TABLE V
THE MEAN I-N RATIO FROM DIFFERENT ROLLING INDENTATION DEPTH

Rolling Indentation	2mm	3mm	4mm	5mm	6mm
Mean IN ratio	0.565	0.528	0.542	0.547	0.515

C. Characterizing the Relationship between the Force and Tissue Deflection

The information contained within the rolling mechanical images can also be used to address another important issue for soft tissue modeling – characterizing the relationship between force and tissue deflection at any location within an organ. Okamura et al [13] used a second order polynomial to fit the force response profile of a needle being inserted into ex-vivo tissue samples (until puncture) for the purpose of modeling needle insertion in soft tissue. It was found that the force-deflection profile of different locations on a liver sample varied significantly as underlying vessels were causing changes in the stiffness distribution, resulting in changing parameter values for the polynomial coefficients. This implies that accurate prediction of how a tissue sample would react to the insertion of needle would require prior information regarding the Force-Deflection characteristic at any point of insertion on that sample.

Such information can be extracted from an assembly of rolling images (i.e. a series of mechanical images taken on the same sample at different wheel indentation depths). By taking a point (x_i,y_i) from the image (representing a point on the sample) and plotting the corresponding force at each of the indentation depths, the Force-Deflection profile for that point can be determined. Experimental results showed that this curve was most accurately described as:

$$F(u) = Cu + Du^2 + Eu^3 \qquad (4)$$

where F is the force, u represents indentation depth, C, D, E are non-negative real numbers. With three unknowns, solving this equation for a point (x_i,y_i) requires the force measurements from three rolling images with different indentation depths, as shown in the following:

$$\begin{bmatrix} C \\ D \\ E \end{bmatrix} = \begin{bmatrix} u_1 & u_1^2 & u_1^3 \\ u_2 & u_2^2 & u_2^3 \\ u_3 & u_3^2 & u_3^3 \end{bmatrix}^{-1} \cdot \begin{bmatrix} \varepsilon f_{u1}(\varepsilon f_{u1} P_1 + P_2) \\ \varepsilon f_{u2}(\varepsilon f_{u2} P_1 + P_2) \\ \varepsilon f_{u3}(\varepsilon f_{u3} P_1 + P_2) \end{bmatrix} \qquad (5)$$

where f_{ui} $(i=1,2,3)$ is the rolling force at the location (x_i,y_i) on the rolling image with an indentation depth u_i . ε_i represents the N/R ratio for u_i. A sample of Force-Deflection profiles from 10 random points on the Liver B is shown in Fig. 11 (u_1=2 mm, u_2=4 mm, u_3=6 mm, ε_i can be found in Table IV). The wide distribution of Force-Deflection profiles in this plot illustrates the highly variable nature of biological soft tissue. It also demonstrates the potential of the rolling mechanical image to provide prior information for the modeling of tool-tissue interactions.

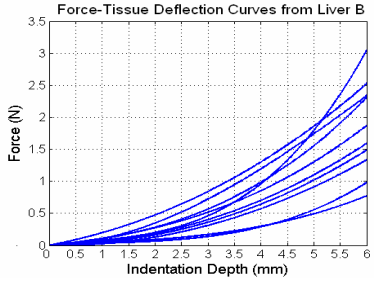

Fig. 11. Ten random force-tissue deflection curves

VIII. Conclusions & Future Work

This paper presented a novel approach for the development of a mechanical image of a soft tissue sample. While the device shows potential to allow a surgeon to extract tissue properties during robot-assisted surgery, many obstacles must be overcome before this becomes a reality. Issues currently under investigation include measuring the actual indentation depth in-vivo and the development of a fibre optic based force sensor with trocar port compatibility. Other potential applications can be identified in the emerging topic of steerable needles. While such devices can be steered through homogenous tissue phantoms, the inherent variability of soft tissue poses difficulties in predicating needle trajectory [17]. One of the factors causing this variability is the changing stiffness distribution in the tissue. We propose that the 'rolling mechanical image' could potentially be used to provide prior information to both aid in the selection of the insertion point for the steerable needle and improve the accuracy of its trajectory prediction.

IX. References

[1] A. E. Kerdok, M. P. Ottensmeyer, R. D. Howe, "Effects of perfusion on the viscoelastic characteristics of liver", *Journal of Biomechanics* , vol. 39(12): 2221-2231, 2005.

[2] F. J. Carter, et al., "Measurements and modeling of the compliance of human and porcine organs", *Med Image Anal*, vol. 5(4): 231-6, 2001.

[3] M.P. Ottensmeyer, "In-vivo measurement of solid organ visco-elastic properties", *Medicine Meets Virtual Reality 02/10, Stud Heatlh Techno Inform*, vol.85: 328-333, 2002.

[4] J.D. Brown, et al., "In-Vivo and In-Situ Compressive Properties of Porcine Abdominal Soft Tissues", *Studies in Health Technology and Informatics - Medicine Meets Virtual Reality*, vol.94:26-32, 2003.

[5] I. Brouwer, et al., "Measuring in-vivo animal soft tissue properties for haptic modeling in surgical simulation", *Studies in Health Technologies and Informatics,* vol. 81: 69-74, 2001.

[6] A. Sarvazyan, "Mechanical imaging: A new technology for medical diagnostics", International Journal of Medical Informatics, vol.49:195–216, 1998.

[7] Parris S. Wellman, et al., "Tactile Imaging of Breast Masses: First Clinical Report", *Arch Surg.* vol.136:204-208, 2001.

[8] V. Egorov, S. Ayrapetyan, and A. P. Sarvazyan, "Prostate Mechanical Imaging: 3-D Image Composition and Feature Calculations", *IEEE Transactions on Medical Imaging*, vol. 25(10): 1329- 1340, 2006.

[9] K.H. Fuchs, "Minimially Invasive Surgery", *Endoscopy*, vol.34: 154-159, 2002.

[10] F. Tendick, M.C. Cavusoglu, "Human Machine Interfaces for Minimally Invasive Surgery", *Proc. 19th Intl. Conference IEEE/EMBS*, pp 2771-277, 1997.

[11] Southern Surgeons Club, "A prospective Analysis of 1518 Laparoscopic Colecystectomies", *New England Journal of Medicine,* vol. 324, pp 1079-1078, 1991.

[12] R.H. Taylor, D. Stioanovici, "Medical Robotics in Computer Integrated Surgery", *IEEE Transactions on Robotics and Automation;* 19(5), 765-781, October 2003.

[13] A. M. Okamura, C. Simone, and M.D. O'Leary, 'Force Modelling for Needle Insertion into Soft Tissue,' *IEEE Transactions on Biomedical Engineering,* Vol. 51, No. 10, pp. 1707-1716, 2004.

[14] M.E. Rentschler, et al., "Modeling, Analysis, and Experimental Study of In Vivo Wheeled Robotic Mobility", *IEEE Transactions on Robotics*, vol.22 (2): 308- 321, 2006.

[15] D. Noonan, et al., "A Dual-Function Wheeled Probe for Tissue Viscoelastic Property Identification during Minimally Invasive Surgery", *Proc IEEE Intl. Conf. Robot. And Automation.,* pp.2629-2634, 2007

[16] H. Liu, et al., "The Development of Nonlinear Viscoelastic Model for the Application of Soft Tissue Identification", accepted *IROS 2007*.

[17] J. M. Romano, et al, "Teleoperation of Steerable Needles", *Proc IEEE Intl. Conf. Robot. And Automation,* pp.934-939, 2007.